Eur. Phys. J. A **6**, 215–223 (1999)

THE EUROPEAN PHYSICAL JOURNAL A

Pion electroproduction in parity violating elastic ep scattering experiment

S. Ong[1], M.P. Rekalo[2,a], J. Van de Wiele[1]

[1] Institut de Physique Nucléaire, IN2P3-CNRS, Université de Paris-Sud, 91406 Orsay Cedex, France
[2] Middle East Technical University, Ankara, Turkey

Received: 20 April 1999 / Revised version: 4 June 1999
Communicated by Th. Walcher

Abstract. This study has been developed for electron-proton scattering experiments when only the scattered electrons are detected. Pion electroproduction on the proton including the cascade $\pi^0 \to 2\gamma$ decay and the QED radiative corrections to elastic ep scattering are investigated. Our results are shown in the kinematical configuration of the parity violating electron scattering experiment planned at the Mainz Microtron (MAMI).

PACS. 25.30.Bf Elastic electron scattering – 13.60.Le Meson production – 13.60.-r Photon and charged-lepton interactions with hadrons

1 Introduction

An experiment to measure parity violating (PV) asymmetries has been performed first at SLAC [1] by deep inelastic electron scattering on deuterium. In the scattering of polarized electrons on unpolarized protons, the measurement of the asymmetry term defined as

$$A_0 = \frac{\sigma(\rightarrow) - \sigma(\leftarrow)}{\sigma(\rightarrow) + \sigma(\leftarrow)} ,$$

due to the interference term between γ and Z^0 graphs, allows one to study the strange contribution to the neutral weak form factors of the proton [2] in the framework of the standard model. For elastic scattering from proton, the expression of A_0 can be expressed in terms of the electromagnetic form factors of the nucleon $G^{p,n}_{E,M}$, the neutral weak vector form factors of the proton $G^Z_{E,M}$ and the neutral weak axial form factor G^Z_A in the following way [2]:

$$A_0 = \left[\frac{-G_F Q^2}{\pi\alpha\sqrt{2}}\right] \times \frac{\epsilon G^p_E G^Z_E + \tau G^p_M G^Z_M - \frac{1}{2}(1-4\sin^2\theta_W)\epsilon' G^p_M G^Z_A}{\epsilon (G^p_E)^2 + \tau (G^p_M)^2} . \quad (1)$$

Where $Q^2 > 0$ is the four momentum transfer, ϵ, ϵ' and τ are kinematic factors, and θ_W is the weak mixing angle. The contribution of the weak axial form factor G^Z_A is suppressed by the factor $(1 - 4\sin^2\theta_W)$.

[a] *Permanent address:* National Science Center, Kharkov Institute of Physics and Technology, Kharkov 310108 Ukraine

The electric and magnetic neutral weak form factors $G^Z_{E,M}$ can be related to the $G^{p,n}_{E,M}$ and the strange quark form factors $G^s_{E,M}$:

$$G^Z_{E,M} = \left(\frac{1}{4} - \sin^2\theta_W\right) G^p_{E,M} - \frac{1}{4} G^n_{E,M} - \frac{1}{4} G^s_{E,M} . \quad (2)$$

The MIT/Bates collaboration [3] report the measurement of the strange $s\bar{s}$ contribution to the magnetic moment of the proton. They obtain the value $G^s_M = 0.23 \pm 0.37 \pm 0.15 \pm 0.19$ n.m. at $Q^2 = 0.1$ (GeV/c)^2.

In recent years, new cw electron accelerators (high intensity, high duty-factor and a polarized beam): TJNAF, AmPS at NIKHEF and MAMI, increase the statistical accuracy for electron-proton scattering experiments more than a factor 10.

In this context, the PVA4 (MAMI) Collaboration proposal [4] is directed towards a measurement of parity violating asymmetries. A total number of elastic events of about 10^{14} is required to measure $A_0 = -8.7\ 10^{-6}$ with $\delta A_0 = 0.05\ A_0$ at a mean four-momentum transfer of $Q^2 = 0.227$ (GeV/c)^2 , assuming a beam polarization of 80%. This would correspond to a measurement of the Dirac form factor $F^s_1(Q^2)$ with $\delta F^s_1 = 0.02 F^s_1$.

Only the scattered electrons are detected in the PVA4 experiment. The radiative correction to elastic scattering and the electroproduction of pions contributions are very important for extracting the tiny asymmetry term with high accuracy. These effects could introduce a background asymmetry [5,6]. An adequate experimental cut of scattered electron energy could isolate the elastic peak from the inelastic contribution, allowing for a discrimination between the background PV asymmetry [6] and the signal.

However, with the special PVA4 detector, an energetic photon coming from $\pi^0 \to \gamma\gamma$ decay can also simulate a scattered electron and increase the inelastic contribution near the elastic peak. In the case of a coincidence electroproduction of pions experiment, a parity conserving asymmetry term has been investigated [5]; this could be a possible source of asymmetry for photons coming from π^0 decay if the cylindrical symmetry of the detector is not perfectly realized.

A full PVA4 detector simulation of the asymmetry term requires a good description for the following chain of processes: $e+p \to e+p+2\gamma$ with production of photon which energy is comparable with the energy of scattered electron in elastic ep scattering. Such processes in principle can produced important background. To estimate such contribution the adequate model for pion electroproduction must be developed. One must include a set of resonances R (Δ or $P_{33}(1232$ MeV), $P_{11}(1440$ MeV), $D_{13}(1520$ MeV) and $S_{11}(1535$ MeV) in the electroproduction of pions model and carefully performs the integral over the electron scattering angles without such natural approximation, as $m_e = 0$, which is typical in consideration of pion electroproduction.

Let us emphasize the two main aspects of this study. In first place we determine an experimental cut of scattered electron energy to isolate the elastic peak from the backgrounds. Secondly, the remaining background asymmetry can be quantified.

The experiment will be performed using the Cherenkov radiator (PbF_2-crystal) to allow a discrimination between elastic scattering and inelastic processes (an energy resolution of $3.3\%/\sqrt{E(GeV)}$ will be achieved). The present study is useful for the total energy deposit simulations at full detector level.

Our paper is organised as follows. In Sect. 2 we develope model for pion photo- and electroproduction wich is goal in the region of πN effective mass from threshold up to second nucleonic resonances. Radiative corrections for the elastic ep-scattering are considered in Sect. 3. The procedure of event generator for the ep-interaction is described in Sect. 4. In Sect. 5 we estimate π^0-electroproduction contribution to the measured cross section in $ep \to e\ (\gamma) + X$ processes and the P-even asymmetry for **ep** collisions with pion production (with subsequent decay $\pi^0 \to 2\gamma$).

2 Electroproduction of pions

There has been considerable activity to measure the pion electroproduction (Fig. 1) in the threshold region (NIKHEF (Amsterdam) [7] and MAMI (Mainz) [8]) to systematically check the Chiral perturbation theory (ChPT) [9].

The energy range of our interest extends from the pion threshold up to the second resonance regions. The ChPT calculations are not applicable in this case ; however many theoretical investigations (unitary isobar model [10], dispersion theoretical analysis [11], dynamical model [12]) describe reasonably available experimental data.

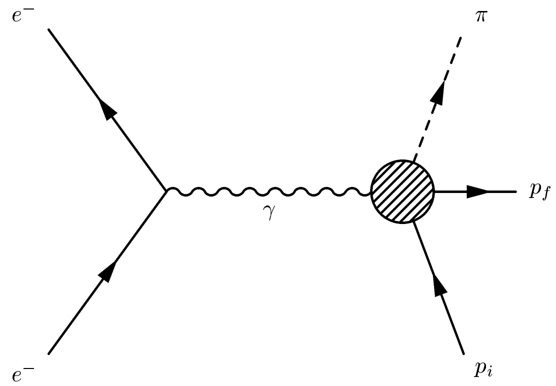

Fig. 1. Pion electroproduction general Feynman diagram

A formalism based on an isobaric approach using Feynman diagrammatic techniques [13], was developed to investigate the charged and neutral pion channels (Fig. 2). The transition vertex $\gamma^* N\Delta$ (γ^* is virtual photon) is decomposed, in analogy with the Dirac-Pauli decomposition of the nucleon electromagnetic current, into the magnetic dipole, electric quadrupole and Coulomb quadrupole [14].

An analysis of pion photo- and electro-production on the nucleon and on nuclei in the Δ region is performed, in the framework of a non-relativistic operator model [15], where both pseudo-scalar and pseudo-vector pion-nucleon couplings are compared.

Recently, a relativistic, gauge invariant and unitary model is investigated in pion photoproduction through the Δ- resonance region [16]. Models for pion photo- and electro-production from threshold up to 1 GeV are available [10,17] The present paper is largely inspired from these previous works [13-17].

The differential cross section for pion production by an incident electron with a helicity h can be written as:

$$\frac{d^3\sigma_h}{dE' d\Omega d\Omega^*_\pi} = \Gamma\ \frac{d\sigma_h}{d\Omega^*_\pi}\ . \tag{3}$$

E' is the energy and Ω the solid angle of the scattered electron in the laboratory frame, while Ω^*_π is the solid angle of the emitted pion in the (π-nucleon) center-of-mass frame. The virtual photon flux Γ represents the probability of the process $e \to e\gamma^*$, it is given by (in the limit $m_e = 0$)

$$\Gamma = \frac{\alpha}{2\pi^2}\frac{E'}{E}\frac{K}{Q^2}\frac{1}{1-\varepsilon}\ . \tag{4}$$

W is the invariant mass of the (π-nucleon) system and $Q^2 = -q^2 = 2EE'(1 - \cos\theta_e)$ the negative four-momentum transfer squared where θ_e is the electron scattering angle. The quantity $\varepsilon = \left(1 + \frac{2|\boldsymbol{q}|^2}{Q^2}\tan^2(\theta_e/2)\right)^{-1}$ characterizes the transverse polarization of the virtual photon and the photon equivalent energy $K = (W^2 - M^2)/2M$ is the laboratory energy necessary for a real photon to excite the hadronic system with mass M to the cm energy W.

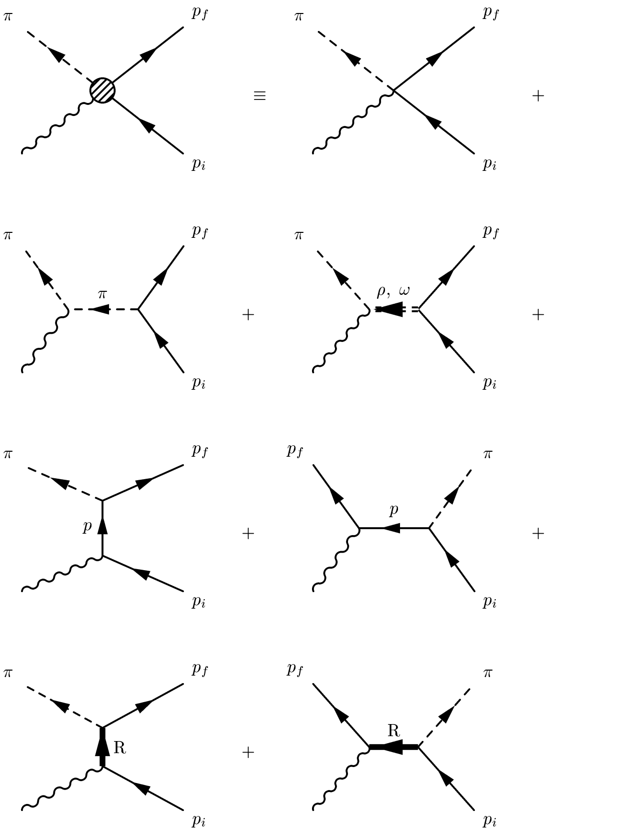

Fig. 2. Feynman diagrams for the virtual photoproduction of one pion: Kroll-Ruderman (contact) diagram, pion pole diagram, vector meson exchange diagram, direct and crossed nucleon Born diagrams, direct and crossed R-resonance diagrams

$d\sigma_h/d\Omega^*_\pi$ is the virtual photoproduction cross section of the process $\gamma^* + N \to N + \pi$ and can be written in the form

$$\frac{d\sigma_h}{d\Omega^*_\pi} = \frac{d\sigma_{unpol}}{d\Omega^*_\pi} + 2h\sqrt{\varepsilon(1-\varepsilon)}\ \frac{d\sigma_e}{d\Omega^*_\pi}\ \sin\phi^*_\pi\ . \tag{5}$$

The unpolarized part can be written as:

$$\frac{d\sigma_{unpol}}{d\Omega^*_\pi} = \frac{d\sigma_T}{d\Omega^*_\pi} + \varepsilon\ \frac{d\sigma_L}{d\Omega^*_\pi} + \varepsilon \frac{d\sigma_{TT}}{d\Omega^*_\pi}\ \cos 2\phi^*_\pi + \sqrt{\varepsilon(1+\varepsilon)}\ \frac{d\sigma_{TL}}{d\Omega^*_\pi}\ \cos\phi^*_\pi\ . \tag{6}$$

where σ_T, σ_L, σ_{TT}, σ_{TL} are respectively the transverse, longitudinal, transverse-transverse interference and transverse-longitudinal interference cross sections. We note that σ_e has the same structure as σ_{TL} except that it is given by the imaginary part of this transverse-longitudinal interference contribution. ϕ^*_π is the azimuthal angle of the $\pi - N$ reaction plane with respect to the electron scattering plane.

To check the consistency of our analysis, comparisons with available experimental data [7,8,18,19,20,21] are necessary. The pion photo- and electro-production on the proton are of great interest as a test of our assumptions on

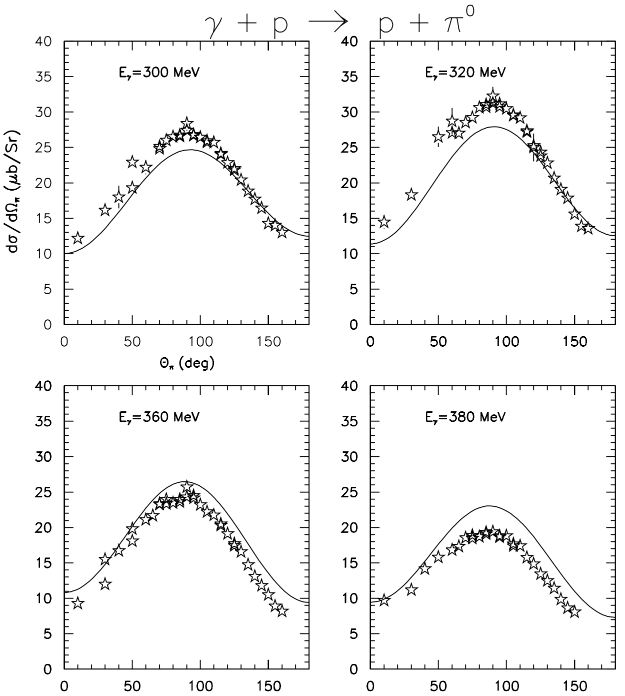

Fig. 3. Differential cross section vs pion c.m. angle for $\gamma p \to \pi^0 p$ reaction. E_γ is the photon energy in Lab. system. Data are taken from [18]

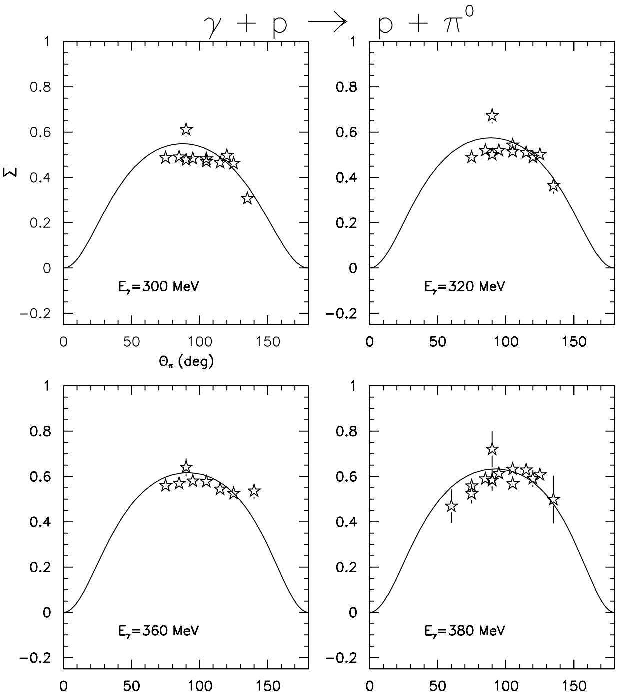

Fig. 4. Photon asymmetry for $\gamma p \to \pi^0 p$ reaction at different photon energies vs pion c.m. angle. Data are taken from [18]

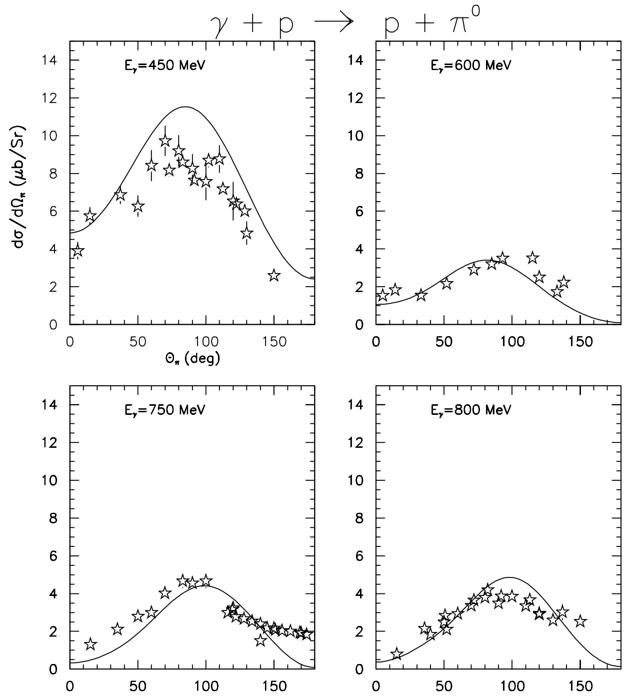

Fig. 5. Same as Fig. 3

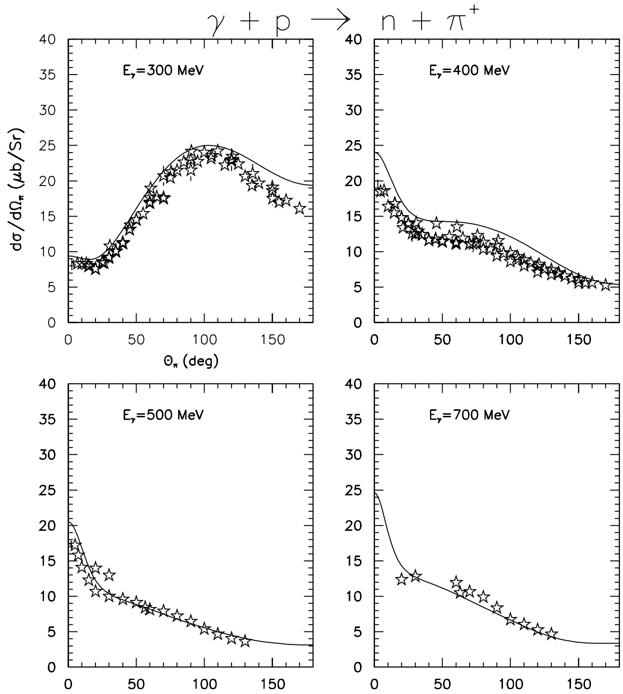

Fig. 7. Differential cross section vs pion c.m. angle for $\gamma p \to \pi^+ n$ reaction. E_γ is the photon energy in Lab. system. Data are taken from [18]

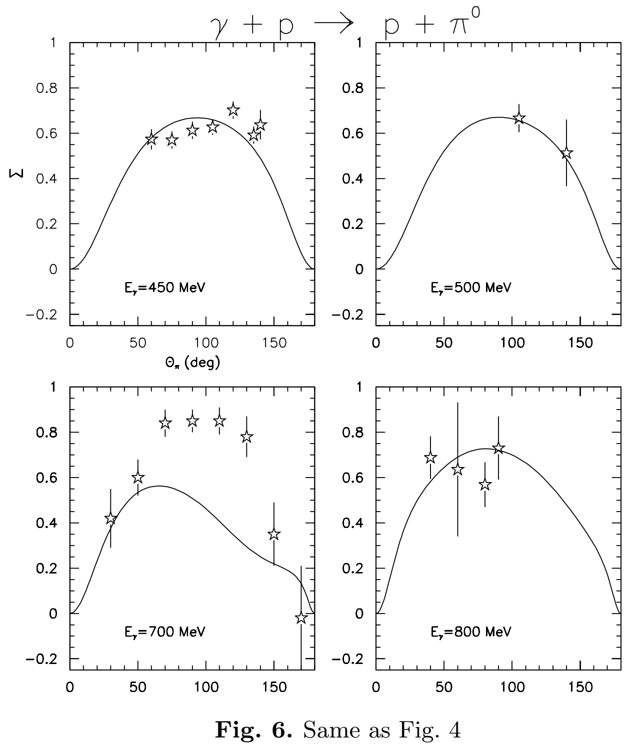

Fig. 6. Same as Fig. 4

the form factors at the γNR vertex and those of the Born terms, the pion-pole and the ρ, ω exchanged diagrams (see Fig. 2).

Our model contains Born terms, vector mesons and nucleon resonances up to the second resonance region ($P_{33}(1232)$, $P_{11}(1440)$, $D_{13}(1520)$ and $S_{11}(1535)$. To implement these resonances, we follow the prescriptions of [17]. And suggested model is satisfied to the gauge invariance of the hadronic electromagnetic interaction. This is especially important to the correct consideration of $e + p \to e + p + \pi^0$ $(\pi^0 \to 2\gamma)$ with detection of only one produced photons when the main contribution to the photon spectrum is due to $Q^2 \simeq 0$.

We use the decay widths of $R \to \pi N$ in order to calculate the πNR strong coupling constants H with the standard procedure. For the spin-$\frac{1}{2}$ resonances:

$$\Gamma_{R\to\pi N}(S_{11}) = \frac{3q_\pi H^2}{2\pi M_R m_\pi^2} \frac{[E_\pi(E+M) + q_\pi^2]^2}{2(E+M)} , \quad (7)$$

$$\Gamma_{R\to\pi N}(P_{11}) = \frac{3q_\pi^3 H^2}{2\pi M_R m_\pi^2} \frac{[E_\pi + E + M]^2}{2(E+M)} . \quad (8)$$

And for the spin-$\frac{3}{2}$ resonances:

$$\Gamma_{R\to\pi N}(P_{33}) = \frac{4q_\pi^3 H^2}{3\pi M_R m_\pi^2}(E+M) , \quad (9)$$

$$\Gamma_{R\to\pi N}(D_{13}) = \frac{4q_\pi^5 H^2}{\pi M_R m_\pi^2} \frac{1}{E+M} . \quad (10)$$

Where q_π is the pion momentum in the πN center of mass system.

$$q_\pi = \sqrt{(M_R^2 - M^2 - m_\pi^2)^2 - 4m_\pi^2 M^2} \;\; /2M_R . \quad (11)$$

E and E_π are the nucleon and pion energies in the same system.

Table 1. Width (in GeV), strong coupling constant, experimental resonance couplings (in GeV$^{-1/2}$) and electromagnetic coupling constants for spin-1/2 resonances

R	Γ	H	$A^p_{1/2}$	$A^n_{1/2}$	G_p	G_n
P_{11}	0.2	0.31	-0.069	0.069	0.272	-0.272
S_{11}	0.12	0.1636	0.073	-0.076	-0.265	0.276

In order to calculate the γNR electromagnetic coupling constant, we use the partial-wave analysis results for resonance couplings A^I_λ ($I = p, n$ and $\lambda = 1/2$ for spin $1/2$; $I = \Delta$ and $\lambda = 1/2,\ 3/2$ for spin 3/2) and each pair of relations:

$$A^{p,n}_{1/2}(S_{11}) = -\frac{1}{\sqrt{2}}\frac{eG_{p,n}}{M}\sqrt{\frac{k}{M(E_1+M)}}\ (M+M_R)\ , \tag{12}$$

$$A^{p,n}_{1/2}(P_{11}) = -\frac{1}{\sqrt{2}}\frac{eG_{p,n}}{M}\sqrt{\frac{k}{M(E_1+M)}}\ (M+M_R)\ , \tag{13}$$

with $E_1 = \sqrt{k^2+M^2}$ and $k = (M_R^2 - M^2)/2M_R$.

$$A^{\Delta}_{1/2}(P_{33}) = -\frac{\sqrt{2}}{3}\frac{ev}{4M}\left[(M_R+M-2k)G_1 - kM_RG_2/M\right]\ , \tag{14}$$

$$A^{\Delta}_{3/2}(P_{33}) = -\sqrt{\frac{2}{3}}\frac{ev}{4M}\left[(M_R+M)G_1 + kM_RG_2/M\right]\ , \tag{15}$$

$$A^{p,n}_{1/2}(D_{13}) = -\frac{1}{\sqrt{3}}\frac{ev}{4M}\left[(M_R+M-2k)G^{p,n}_1 + M_RG^{p,n}_2(M_R+M-k)/M\right]\ , \tag{16}$$

$$A^{p,n}_{3/2}(D_{13}) = -\frac{ev}{4M}\left[(M_R+M)G^{p,n}_1 + M_RG^{p,n}_2(M_R+M-k)/M\right]\ , \tag{17}$$

with

$$v = \sqrt{\frac{k}{M(M_R+M-k)}}\ . \tag{18}$$

The coupling constants $G_{1,2}$ and $G^{p,n}_{1,2}$ used in [17] can be obtained from (12-18). In summary, we display in Tables [1-3] the numerical values of these differents coupling constants.

The Δ propagator is not as well defined as the nucleon one [22], we assume, in this study, the Rarita-Schwinger formalism [23] for treating the spin 3/2 particle and we use the on-shell form of the propagator.

The photon asymmetry is an important polarization observable for pion photoproduction that we can used to check our model. This photon asymmetry Σ is defined by

$$\Sigma = \frac{\sigma_\perp - \sigma_\parallel}{\sigma_\perp + \sigma_\parallel}\ . \tag{19}$$

Table 2. Width (in GeV) and experimental values of the resonance couplings (in GeV$^{-1/2}$) for spin-3/2 resonances

R	Γ	$A^p_{1/2}$	$(A^\Delta_{1/2})$	$A^n_{1/2}$	$A^p_{3/2}$	$(A^\Delta_{3/2})$	$A^n_{3/2}$
P_{33}	0.109		(-0.133)			(-0.244)	
D_{13}	0.140	-0.022		-0.065	0.167		-0.144

Table 3. Strong and electromagnetic coupling constants for spin-3/2 resonances

R	H	G^p_1	(G_1)	G^n_1	G^p_2	(G_2)	G^n_2
P_{33}	0.585		(5.107)			(-3.06)	
D_{13}	0.428	-5.57		0.853	2.97		0.475

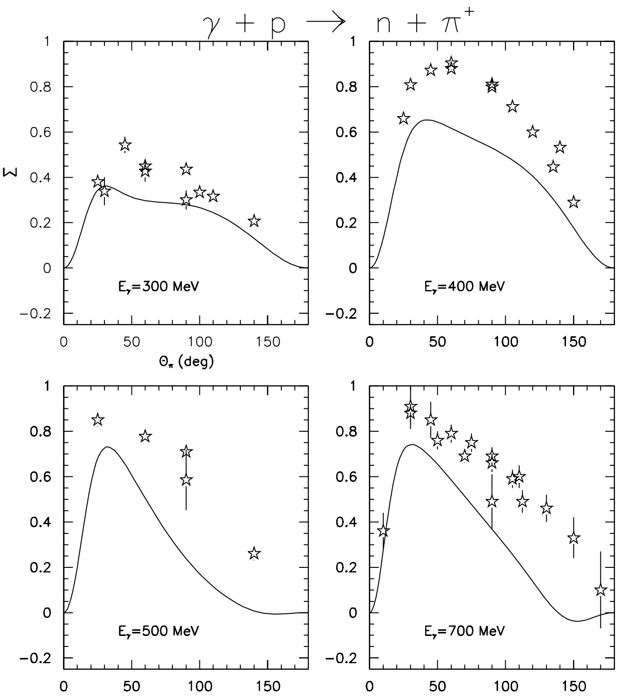

Fig. 8. Photon asymmetry for $\gamma p \to \pi^+ n$ reaction at different photon energies vs pion c.m. angle. Data are taken from [18]

where $\sigma_\perp$ and $\sigma_\parallel$ are the differential cross sections for photon polarization perpendicular and parallel to the pion production plane.

A comparison between our predictions and the existing experimental data are display in Figs [3-9]. It can be seen that a good agreement with the data is obtained for different kinematical regions.

3 Radiative corrections to elastic scattering

We investigate the QED radiative corrections based on the previous work of Mo and Tsai [24]. The higher-order Feynman diagrams used in the calculation of the radiative corrections are displayed in Fig. 10. It is assumed that the

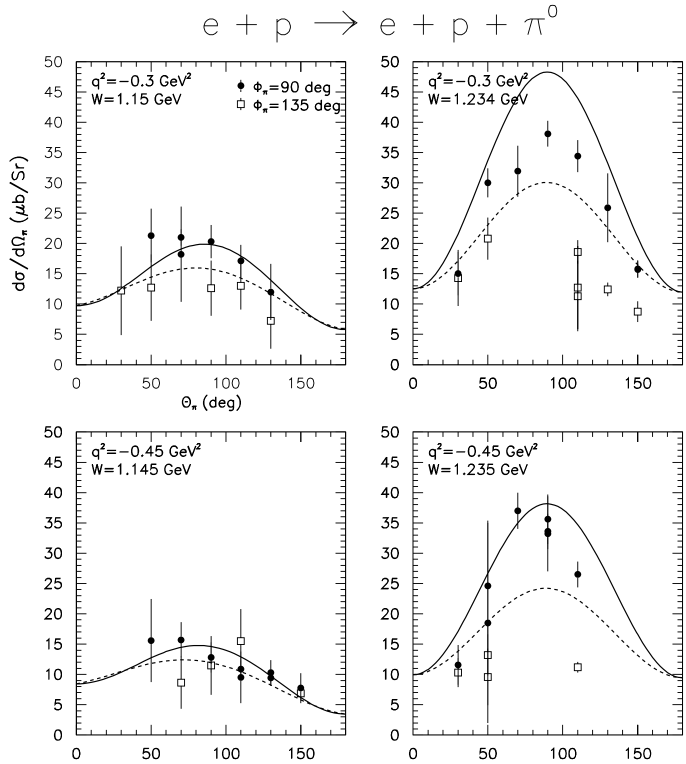

Fig. 9. The θ_π dependence of the differential cross section for $p(e, e'\pi^0)p$ and for $\epsilon = 0.97$. The solid and dashed curves are obtained for $\phi^*_\pi = 90$ and 135 degrees respectively. Data are taken from [19]

radiative corrections at the proton vertex is small, thus we neglect this contribution in our calculation.

In principle one might consider the electroweak radiative corrections in PV experiment, in the framework of the standard model, to be applied to the neutral weak form factors of the proton. The expression of $G^Z_{E,M}$ in (2) must be modified in the following form [25]:

$$G^Z_{E,M} = \left(\frac{1}{4} - \sin^2\theta_W\right)[1 + R^p_V]G^p_{E,M} - \frac{1}{4}[1 + R^n_V]G^n_{E,M} - \frac{1}{4}[1 + R^s_V]G^s_{E,M}. \quad (20)$$

The factors R^i_V are weak radiative corrections, which have been computed in [25].

The QED radiative corrections depend on the kinematics of the scattering. The radiative tail contributes down to values of E' where other background processes (π production, Δ-resonance, etc...) occur. The radiative tail from the elastic peak is taken into account up to the Δ-resonance region, allowing one to isolate the pion-electroproduction channels. It was shown by Mo and Tsai [24], that the radiative tail from the elastic peak, can be computed with good accuracy assuming the peaking approximation. The initial radiation (photon emitted by the incident electron) contribution is independent of the final radiation (photon emitted by the scattered electron)

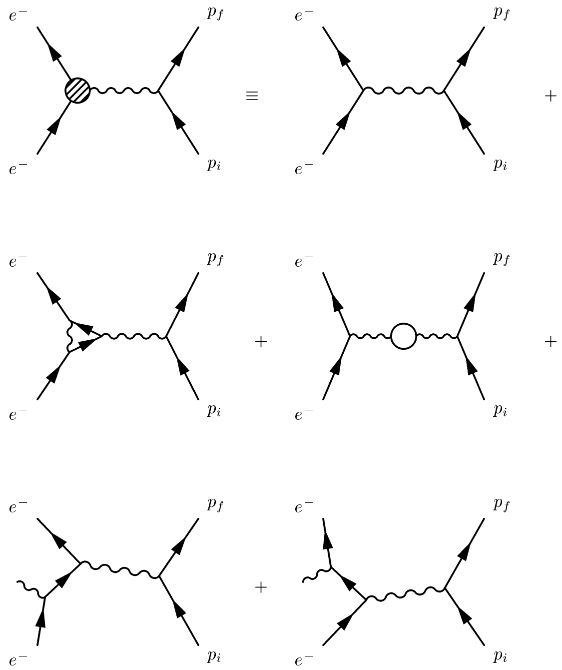

Fig. 10. Feynman diagrams used in the calculation of the radiative corrections: elastic, vertex part, vacuum polarization, initial radiation and final radiation

when the electron is scattered at sufficiently large angle ; in our investigation we neglect the interference between the initial and final radiations.

The radiative tail cross section can be written as:

$$\frac{d\sigma_r}{d\Omega dE'}(\omega > \Delta E) = \frac{d\sigma_{ini.}}{d\Omega dE'}(\omega > \Delta E) + \frac{d\sigma_{fin.}}{d\Omega dE'}(\omega > \Delta E). \quad (21)$$

The two terms in (21) represent respectively the initial and final radiation contributions. ω is the photon energy emitted, and ΔE is a cut-off energy in defining the peak of elastically scattered electrons. The integration from $\omega = 0$ to ΔE plus the vacuum polarization and the vertex correction are already taken into account in the corrected elastic cross section in the form:

$$(1 + \delta)\frac{d\sigma_0}{d\Omega} , \quad (22)$$

where

$$\frac{d\sigma_0}{d\Omega} = \frac{\alpha^2 E'^2}{Q^4}\frac{4\cos^2(\theta/2)}{[1 + 2(E/M)\sin^2(\theta/2)]} \times \left(\frac{G^2_E + \tau G^2_M}{1 + \tau} + 2\tau\tan^2(\theta/2)G^2_M\right). \quad (23)$$

with $\tau = Q^2/4M^2$. The magnetic and electric form factors of the proton G_M and G_E used in the calculation are

$$G_E(Q^2) = \frac{1}{(1 + Q^2/0.71)^2} , \quad (24)$$

$$G_M(Q^2) = 2.793\ G_E(Q^2). \tag{25}$$

The δ term is given by

$$\delta = -\frac{\alpha}{\pi}\left[\frac{28}{9} - \frac{13}{6}\ln\frac{Q^2}{m^2} + [\ln(E/\Delta E) + \ln(E'/\Delta E)]\left(\ln\frac{Q^2}{m^2} - 1\right) - \Phi\left(-\frac{E-E'}{E'}\right) - \Phi\left(\frac{E-E'}{E}\right)\right], \tag{26}$$

with the Spence function:

$$\Phi(x) = -\int_0^x \frac{\ln|1-y|}{y}\ dy\ .$$

Finally, the radiative tail from the elastic peak (ignoring the straggling), in the peaking approximation, is given by [24]:

$$\frac{d\sigma_r}{d\Omega dE'} = \frac{t_s}{\omega_s}\ \frac{M + (E-\omega_s)(1-\cos\theta)}{M - E'(1-\cos\theta)} \times \frac{d\sigma_0(E-\omega_s)}{d\Omega} + \frac{t_p}{\omega_p}\frac{d\sigma_0(E)}{d\Omega}, \tag{27}$$

with

$$\omega_s = \frac{-Q^2 + 2M(E-E')}{2[M - E'(1-\cos\theta)]}\ , \tag{28}$$

$$\omega_p = \frac{-Q^2 + 2M(E-E')}{2[M + E(1-\cos\theta)]}\ , \tag{29}$$

$$x_s = \frac{E-\omega_s}{E}\ , \tag{30}$$

$$x_p = \frac{E'}{E'+\omega_p}\ , \tag{31}$$

$$X_s = 2(E-\omega_s)E'(1-\cos\theta)\ , \tag{32}$$

$$X_p = 2EE'(1-\cos\theta)\ , \tag{33}$$

$$t_s = \frac{\alpha}{\pi}\left[\frac{1+x_s^2}{2}\ln\frac{X_s}{m^2} - x_s\right]\ , \tag{34}$$

$$t_p = \frac{\alpha}{\pi}\left[\frac{1+x_p^2}{2}\ln\frac{X_p}{m^2} - x_p\right]\ . \tag{35}$$

ω_s and ω_p are the photon energies along the incident and outgoing electron directions.

The PVA4 detector accumulates the energy of the electron and of the photon emitted in the same direction. Therefore, we neglect the final radiation term in this study.

4 Event generator

The experimental spectrum between $30^0 \leq \theta \leq 40^0$ shows a large elastic peak [26] with some additional events above the π threshold. This background could provide from photons due to π^0 decay or π^+ hitting the detector. Some Monte Carlo simulations [27] have shown that it is very hard to discriminate between Čerenkov light of electrons and photons at the same energy while the Čerenkov radiation of π^+ in the PbF2 detector contributes to the spectrum at lower energy.

An event generator for *ep* reaction has been performed to study in more details both the inclusive electron and the background spectra. In the case of a coincidence experiment, the differential cross section can be written, using the spherical harmonics, in the following form:

$$\frac{d^3\sigma_h(E',\Omega_e,\Omega_\pi^*)}{dE'd\Omega d\Omega_\pi^*} = \sum_\ell \Big(\ A^R_{\ell\ 0}(h)\ Y_\ell^0(\theta_\pi^*,\phi_\pi^*=0) + 2\sum_{m>0} Y_\ell^m(\theta_\pi^*,\phi_\pi^*=0) \times [A^R_{\ell\ m}(h)\cos(m\phi_\pi^*) - A^I_{\ell\ m}(h)\sin(m\phi_\pi^*)]\Big). \tag{36}$$

$$A_{\ell\ m}(h) \equiv A_{\ell\ m}(h, E', \Omega_e)\ . \tag{37}$$

$$A_{\ell\ m}(h) = A^R_{\ell\ m}(h) + \imath\ A^I_{\ell\ m}(h)\ . \tag{38}$$

$$A^R_{\ell m}(h) = \int_0^\pi Y_\ell^m(\theta_\pi^*,\phi_\pi^*=0)\sin(\theta_\pi^*)d\theta_\pi^* \times \int_0^{2\pi}\frac{d^3\sigma_h(E',\Omega_e,\Omega_\pi^*)}{dE'd\Omega d\Omega_\pi^*}\cos(m\phi_\pi^*)d\phi_\pi^*, \tag{39}$$

$$A^I_{\ell m}(h) = -\int_0^\pi Y_\ell^m(\theta_\pi^*,\phi_\pi^*=0)\sin(\theta_\pi^*)d\theta_\pi^* \times \int_0^{2\pi}\frac{d^3\sigma_h(E',\Omega_e,\Omega_\pi^*)}{dE'd\Omega d\Omega_\pi^*}\sin(m\phi_\pi^*)d\phi_\pi^*. \tag{40}$$

From equations (3,5-6), we obtain:

$$A^R_{\ell\ m}(h) = A^R_{\ell\ m}(-h)\ , \tag{41}$$

$$A^I_{\ell\ m}(h) = -A^I_{\ell\ m}(-h)\ , \tag{42}$$

$$A^I_{\ell\ 0}(h) = 0\ , \tag{43}$$

$$A^I_{\ell\ 2}(h) = 0\ , \tag{44}$$

$$A_{\ell\ m}(h) = 0 \quad \text{if } m > 2\ . \tag{45}$$

These equations show that only the values of $A_{\ell\ m}(h = 1/2)$ are needed to get the observables with $h = \pm 1/2$.

We are able to reproduce the correct value of the cross section, in different kinematic configurations, using $A_{\ell\ m}$ parameters with $\ell \leq 10$ for π^0 channel and $\ell \leq 20$ for charged channel in a coincidence experiment. Let us notice that only the $A_{0\ 0}$ term is needed to reproduce the differential cross section in an inclusive reaction.

Let us describe now the main features of the Monte Carlo:

– The scattered electrons are generated according to the cross sections ((23) for the elastic channel, (27) for the radiative tail and (36) for the pion channel).
– The limits of parameters to be generated are according to the experimental acceptance.

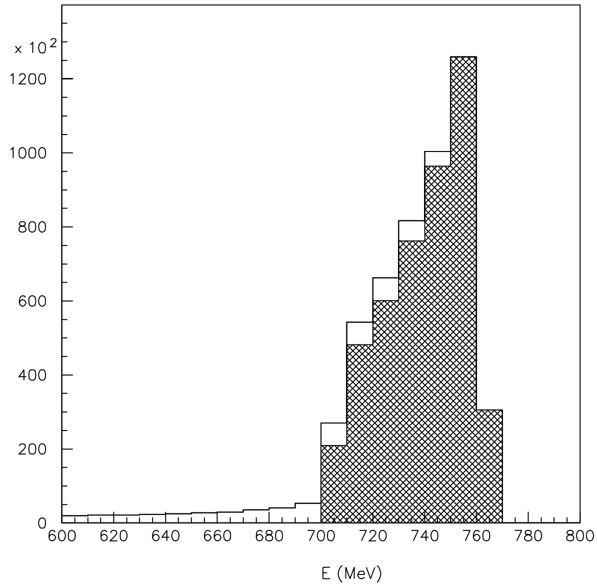

Fig. 11. Number of events generated in *ep* scattering vs scattered electron energy with $E_{beam} = 855$ MeV and $30^0 \leq \theta_e \leq 40^0$: elastic peak (hatched histogram) and elastic peak including radiative corrections.

– The four-momenta of all particles are determined in various frames (Lab., $\pi - N$ cm.), thanks to rotations and Lorentz boosts.

This program gives absolute normalization and generates individual events. Various distributions can be extracted from theses weighted events.

5 Numerical results

In this section, we discuss the results of our generator of events. We display in Fig. 11, the corrected elastic peak including radiative corrections. This effect is under control and we are going to discuss the background asymmetry contamination by photons. This contamination is expressed by:

$$A = A_0 \frac{1 + \dfrac{S_{ph}}{S_0}\dfrac{A_{ph}}{A_0}}{1 + \dfrac{S_{ph}}{S_0}} \, . \tag{46}$$

Where S_0 and S_{ph} are respectively the number of elastic electrons and photons emitted in the angular region $30^0 \leq \theta_e(\theta_\gamma) \leq 40^0$ of PVA4 (MAMI) detector with an energy range 600 MeV $\leq E' \leq$ 800 MeV. $A_0 = -8.7\ 10^{-6}$ and A_{ph} are respectively the PV asymmetry term which we would like to measure and the conserving parity background asymmetry. A relatively large number of S_{ph} is required to get a reasonable value of the A_{ph} with a good confidence level.

To visualize the rate S_{ph}/S_0 in (46), we display in Fig. 12, the number of photons (multiplied by 100) and electrons detected in the same energy and angular ranges

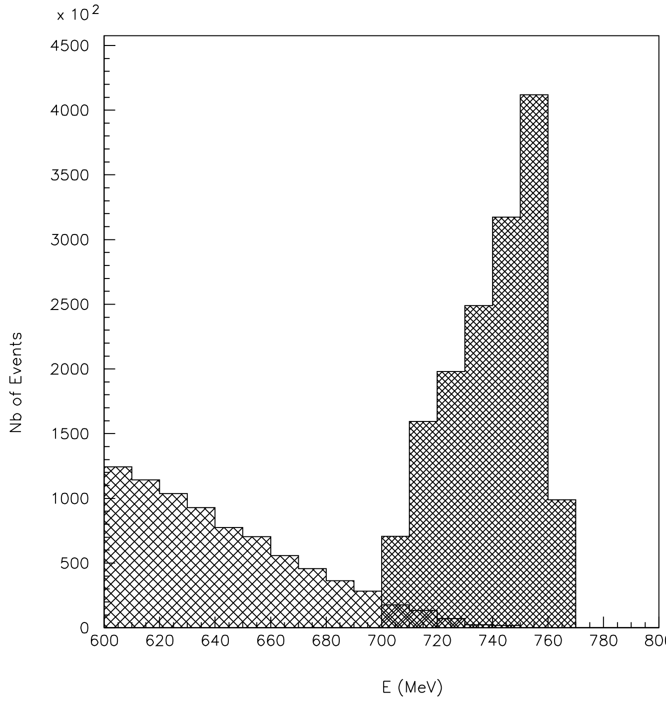

Fig. 12. Number of events generated in *ep* scattering vs scattered electron energy with $E_{beam} = 855$ MeV and $30^0 \leq \theta_e(\theta_\gamma) \leq 40^0$ for elastic peak (small crosshatched histogram); photons (x 100) coming from $\pi^0 \to 2\gamma$ decay (large crosshatched histogram)

(with 2 10^7 generated events). The low energy part of the elastic E'-spectrum is modified near the elastic peak due to the cascade $e{+}p \to e{+}p{+}\pi^0 \to e{+}p{+}\gamma\gamma$ processes. For 10^7 events generated, one obtains $\approx$7.5 10^5 elastic events and $\approx$1.6 10^6 photon events coming from π^0 decays which can simulate scattered electrons in an energy range $E' \leq$ 800 MeV and $30^0 \leq \theta_e(\theta_\gamma) \leq 40^0$. Let us notice that the elastic channel is dominated by the inelastic one due to the integral over the electron scattering angles.

This contamination is estimated to be small (S_{ph}/S_0 =0.4 %) in the critical region 620 MeV $\leq E' \leq$ 800 MeV.

The photon asymmetry is defined as:

$$A_{ph} = \frac{N_{\gamma_+} - N_{\gamma_-}}{N_{\gamma_+} + N_{\gamma_-}} \, , \tag{47}$$

where $N_{\gamma_\pm}$ are respectively number of photons produced by polarized electrons with $h = \pm 1/2$ and can be computed from π^0 electroproduction cross section given by (36).

For 2 10^7 generated events, we obtain $A \simeq A_0(1{+}0.01)$ This indicates a small contamination to the A_0 asymmetry. If the energy cut is achieved at higher value ($E' \approx 640$ MeV), or if the statistic is improved, this contamination becomes smaller and we conclude that the photon background does not affect in a significant way the PVA4 measurement. This study can be used to calculate the contribution of different geometrical false asymmetries on systematical errors.

6 Conclusions

Let us summarize here the main result of our analysis. We developed a model for pion photo and electroproduction which is adequate for description of necessary observables up to $E_\gamma \simeq 800$ MeV.

For accurate calculation of photon spectra from chain of reaction $e + p \to e + p + \pi^0 \to e + p + \gamma\gamma$ the corresponding formalism is suggested, with special attention to very small Q. The gauge invariance for the electromagnetic current as well as exact consideration of effects with non zero electron mass are very important here.

We demonstrated that γ-contribution from π^0 electroproduction is not dangerous for the condition of planning (running) Mainz parity violating experiment. On the basis of our analysis the event generator for ep scattering can be performed.

Recently, Happex Collaboration [28] report the measurement of the PV asymmetry at $Q^2 = 0.48$ (GeV/c)^2:

$$G_E^s + 0.39 G_M^s = 0.023 \pm 0.034(stat.) \pm 0.022(syst.) \\ \pm 0.026(\delta G_E^n) \ .$$

The strange quark contribution to this asymmetry is very small, a value compatible with vanishing strangeness contributions. It is very important to check this result by another measurement (PVA4 or G0 [29] at TJNAF).

For backward angle ep scattering experiment planned at G0, our generator can be used with appropriated kinematical parameters.

The authors are grateful to M. Vanderhaeghen for useful discussions. We would like to thank the PVA4 Collaboration members for constructive remarks and constant encouragements.

References

1. C.Y. Prescott et al. Phys. Lett. **B77**, 347 (1978); ibid. **B84**, 524 (1979)
2. M.J. Musolf et al., Phys. Rep. **239**, 1 (1994)
3. B. Mueller et al., Phys. Rev. Lett. **78**, 3824 (1997)
4. Mainz proposal A4/1-93 (1993), spokeesperson: D.v. Harrach; E. Heinen-Konschak, Doctoral thesis, Mainz University (1994)
5. S. Nozawa and T.S.H. Lee, Nucl. Phys. **A513**, 543 (1990)
6. L.M. Nath, K. Schilcher and M. Kretzschmar, Phys. Rev. **D25**, 2300 (1982); H.W. Hammer and D. Drechsel, Z. Phys. **A353**, 321 (1995)
7. H.B. van den Brink et al., Phys. Rev. Lett. **74**, 3561 (1995)
8. A. Richter, Doctoral thesis, Mainz University (1994); M. Distler, Doctoral thesis, Mainz University (1996); R. Beck et al., Phys. Rev. Lett. **78**, 606 (1997)
9. V. Bernard, N. Kaiser, T.S.H. Lee and U.G. Meißner, Phys. Rep. **246**, 315 (1994); V. Bernard, N. Kaiser, and U.G. Meißner, Int. J. Mod. Phys. **E4**, 193 (1995); G. Ecker, Prog. Nucl. Part. Phys. **35**, 1 (1995)
10. D. Drechsel, O. Hanstein, S.S. Kamalov and L. Tiator, Nucl. Phys. **A645**, 145 (1999)
11. O. Hanstein, D. Drechsel and L. Tiator, Phys. Lett. **B385**, 45 (1996); ibid. **B399**, 13 (1997); L. Tiator, nucl-th/9710036 (1997)
12. S. Nozawa and T.S.H. Lee, Nucl. Phys. **A513**, 511 (1990)
13. G. Cochard, M. Karatchentzeff, P. Kessler and B. Roehner, Il Nuovo cimento **12A**, 909 (1972)
14. H.F. Jones and M.D. Scadron, Ann. of Phys. **81**, 1 (1973)
15. I. Blomqvist and J.M. Laget, Nucl. Phys. **A280**, 405 (1977); J.M. Laget, Nucl. Phys. **A481**, 765 (1988)
16. M. Vanderhaeghen, K. Heyde, J. Ryckebusch and M. Waroquier, Nucl. Phys. **A595**, 219 (1995) and references therein.
17. H. Garcilazo and E. Moya de Guerra, Nucl. Phys. **A562**, 521 (1993)
18. Pion Photoproduction Database in SAID program, http://said.phys.vt.edu/
19. R. Siddle et al., Nucl. Phys. **B35**, 93 (1971)
20. H. Breuker et al., Nucl. Phys. **B146**, 285 (1978)
21. R. Neuhausen, Nucl. Phys. **B44**, 695 (1995); K.I. Blomqvist et al., Z. Phys. **A353**, 415 (1996)
22. H.T. Williams, Phys. Rev. **C31**, 2297 (1985)
23. W. Rarita and J. Schwinger, Phys. Rev. **60**, 61 (1941)
24. L.W. Mo and Y.S. Tsai, Rev. of Mod. Phys. **41**, 205 (1969)
25. M.J. Musolf and B.R. Holstein, Phys. Lett. **B242**, 461 (1990)
26. F.E. Mass et al., in proceedings of the Spin 96, Amsterdam (1996), World Scientific, p.438.
27. L.H. Rosier (private communication)
28. K.A. Aniol et al., Happex Coll., Phys. Rev. Lett. **82**, 1096 (1999); C. Cavata, Joliot Curie school, September 1998.
29. PAC Jeopardy Proposal, The G0 Experiment (Originally E91-017)-The G0 Collaboration, December 16, 1998 (G0 Internal Report G0-98-036)